

Comparative Study of CuMoO₄ Electrodes Synthesized Using DMSO and NMP: Morphological and Electrochemical Insights

Asiye Altan^{1,a}, Fatma Kılıç Dokan^{2,b,*}, Mustafa Serdar Onses^{3,c}, Ertuğrul Şahmetlioğlu^{4,d}

¹Department of Computational Science and Engineering, Graduate School of Natural and Applied Sciences, Kayseri University, Kayseri, Türkiye.

²Department of Chemistry and Chemical Processing Technologies, Mustafa Çıkrıkcıoğlu Vocational School, Kayseri University, Kayseri, Türkiye.

³Department of Materials Science and Engineering, Faculty of Engineering, Erciyes University, 38039, Kayseri, Türkiye.

⁴Department of Basic Sciences of Engineering, Kayseri University, 38039, Kayseri, Türkiye.

*Corresponding author e-mail address: fatmakilic@kayseri.edu.tr

Research Article

History

Received: 16.06.2025

Accepted: 14.05.2026

ABSTRACT


This study presents a systematic comparison of CuMoO₄ electrodes synthesized using dimethyl sulfoxide (DMSO) and N-methyl-2-pyrrolidone (NMP) as solvent media, with emphasis on their structural and electrochemical performance for supercapacitor applications. Both solvents enable the formation of crystalline CuMoO₄; however, distinct differences in morphology and electrochemical behavior are observed. The DMSO-derived electrode exhibits a more porous and homogeneous structure, facilitating enhanced electrolyte accessibility and ion transport. As a result, it delivers a high specific capacitance of 549.6 F g⁻¹ at 1 A g⁻¹, significantly outperforming the NMP-based electrode (266 F g⁻¹ at 1 A g⁻¹). Even at elevated current densities, the DMSO electrode maintains a capacitance of 323 F g⁻¹ at 20 A g⁻¹, indicating superior rate capability. Electrochemical impedance spectroscopy reveals reduced charge transfer resistance and improved ion diffusion kinetics for the DMSO-derived electrode, which is attributed to improved electrode architecture and enhanced electronic pathways. Furthermore, the DMSO-based system demonstrates better cycling stability compared to the NMP counterpart, maintaining consistent electrochemical performance over repeated cycles. The comparable voltage windows observed in cyclic voltammetry and galvanostatic charge-discharge profiles confirm stable operation, while the improved performance is linked to more efficient utilization of electroactive sites. The findings demonstrate that solvent selection plays a decisive role in tailoring the structural and electrochemical properties of CuMoO₄ electrodes. DMSO-assisted synthesis enables the formation of a more favorable electrode architecture, resulting in enhanced capacitance, rate capability, and stability. This study highlights solvent engineering as an effective strategy for optimizing electrode materials in advanced supercapacitor systems.

Keywords: Copper molybdate, Electrochemical energy storage, Supercapacitor




This article is licensed under a Creative Commons Attribution-NonCommercial 4.0 International License (CC BY-NC 4.0)

^a  0009-0007-1155-0859

^c  0000-0001-6898-7700

^b  0000-0002-5355-2904

^d  0000-0002-7324-0385

1. Introduction

Supercapacitors have emerged as one of the most promising energy storage devices due to their high power density, rapid charge-discharge cycles, and exceptional cycle stability. These characteristics make them particularly suitable for applications requiring quick bursts of energy, such as in electric vehicles, renewable energy systems, and consumer electronics. However, one of the key limitations of supercapacitors is their relatively low energy density compared to traditional batteries, which restricts their ability to store large amounts of energy for extended periods. To overcome this limitation, researchers have focused on improving the performance of supercapacitors by developing advanced electrode materials capable of offering high specific capacitance, superior conductivity, and excellent electrochemical stability[1-7].

The role of electrode materials in supercapacitors cannot be overstated, as they are directly responsible for the energy storage capacity, charge/discharge rates, and

long-term stability of the devices. While carbon-based materials such as activated carbon, graphene, and carbon nanotubes have traditionally been the primary choice for supercapacitors, these materials often face limitations in terms of their pseudocapacitance, which limits their overall energy storage performance. This has driven the search for alternative materials with superior electrochemical properties. Among these alternatives, metal-based compounds, particularly metal molybdates such as CuMoO₄, have shown great promise due to their unique properties, including high specific capacitance, excellent conductivity, and good electrochemical stability[8,9].

CuMoO₄ has emerged as a highly promising candidate for next-generation supercapacitor electrodes due to its exceptional electrochemical characteristics, including high specific capacitance, fast charge-discharge dynamics, chemical stability, and electrical conductivity. Among various transition metal molybdates, CuMoO₄

uniquely combines the redox activity of copper ions with the structural stability offered by the molybdate framework, enabling both faradaic and non-faradaic energy storage mechanisms to coexist synergistically. One of the most significant advantages of CuMoO_4 is its ability to facilitate rapid redox reactions, which supports quick energy uptake and release, a critical requirement in high-power applications such as regenerative braking systems, portable electronics, and backup power sources[10-15]. The presence of copper in the +2 oxidation state contributes to reversible redox transitions, which enhances pseudocapacitive behavior and improves charge storage capability beyond that of conventional double-layer capacitors. Moreover, the material demonstrates excellent electrochemical cycling stability, maintaining a significant portion of its initial capacitance over prolonged charge-discharge cycles. This ensures long-term durability, making CuMoO_4 not only efficient but also reliable under repeated operational conditions. Its relatively high electrical conductivity aids in minimizing internal resistance, thus lowering energy loss and improving coulombic efficiency. In addition, the morphology and structure of CuMoO_4 can be tuned through different synthesis routes and solvent systems, which greatly influences its surface area, porosity, and ion transport kinetics. For instance, when prepared using DMSO as a solvent, CuMoO_4 exhibits improved film homogeneity and ion diffusion, leading to enhanced electrochemical performance compared to samples synthesized using NMP, as confirmed by CV, GCD, and EIS analyses[16-19]. The results from this study underline the importance of the synthesis environment in optimizing electrode properties[20].

Collectively, these findings reinforce the role of CuMoO_4 as an advanced electrode material capable of balancing high energy and power densities a balance often difficult to achieve in electrochemical energy storage. As the demand for sustainable and efficient energy storage systems continues to grow, CuMoO_4 -based electrodes stand out as strong contenders for integration into modern supercapacitor technologies. Previous studies have demonstrated that CuMoO_4 exhibits promising electrochemical properties such as high specific capacitance, excellent conductivity, and good cycling stability, making it a strong candidate for supercapacitor applications. However, the impact of synthesis conditions, particularly the choice of solvent, on the morphological and electrochemical performance of CuMoO_4 electrodes has not been fully explored. This study focuses on a comparative investigation of CuMoO_4 electrodes synthesized using two different solvents, dimethyl sulfoxide (DMSO) and N-methyl-2-pyrrolidone (NMP). Solvent selection plays a decisive role in hydrothermal and solvothermal synthesis processes, as physicochemical properties such as dielectric constant, viscosity, polarity, and boiling point directly influence nucleation kinetics and crystal growth behavior. Solvents with higher dielectric constants enhance ionic dissociation and facilitate homogeneous precursor distribution, which can promote

uniform crystal formation and increased porosity. Dimethyl sulfoxide (DMSO), with a dielectric constant of approximately 46.7 and strong coordinating ability, is expected to improve precursor solubility and regulate crystal growth. In contrast, N-methyl-2-pyrrolidone (NMP), possessing a comparatively lower dielectric constant (~32) and different solvation dynamics, may lead to variations in diffusion kinetics and particle aggregation. Based on these physicochemical differences, it was hypothesized that DMSO would promote the formation of a more porous and electrochemically favorable CuMoO_4 architecture compared to NMP. However, a systematic evaluation of solvent-dependent structural evolution in CuMoO_4 remains insufficiently explored. The aim is to understand how these solvents influence the structural properties, surface morphology, and electrochemical behavior of CuMoO_4 , thereby affecting its performance as an electrode material in supercapacitors[21-22].

By systematically analyzing the morphological characteristics through advanced imaging techniques and evaluating the electrochemical performance using cyclic voltammetry (CV), galvanostatic charge-discharge (GCD), and electrochemical impedance spectroscopy (EIS), this work provides detailed insights into the effects of solvent choice on CuMoO_4 electrodes. The findings offer critical information on optimizing electrode fabrication processes to enhance energy storage capacity, power density, and cycling stability.

Overall, this study aims to advance the understanding of CuMoO_4 as a supercapacitor electrode material and to highlight the significance of solvent selection in synthesizing electrodes with superior electrochemical properties. These insights contribute to the development of more efficient, sustainable, and high-performance energy storage devices suitable for renewable energy applications.

2. Materials and Methods

2.1. Materials

Copper (II) chloride dihydrate ($\text{CuCl}_2 \cdot 2\text{H}_2\text{O}$), cobalt (II) nitrate hexahydrate ($\text{Co}(\text{NO}_3)_2 \cdot 6\text{H}_2\text{O}$), nickel (II) nitrate hexahydrate ($\text{Ni}(\text{NO}_3)_2 \cdot 6\text{H}_2\text{O}$), ammonium heptamolybdate tetrahydrate ($(\text{NH}_4)_6\text{Mo}_7\text{O}_{24} \cdot 4\text{H}_2\text{O}$), potassium hydroxide (KOH), urea ($\text{CH}_4\text{N}_2\text{O}$), N-methyl-2-pyrrolidone (NMP), and dimethyl sulfoxide (DMSO) were obtained from MERCK. Graphite, polyvinylidene fluoride (PVDF), and ethanol ($\text{C}_2\text{H}_6\text{O}$) were supplied by SIGMA-ALDRICH, while the nickel foam was purchased from MTI KOREA.

2.2. Synthesis of CuMoO_4

CuMoO_4 was synthesized following a method adapted from the literature. To achieve a 1:1 Cu:Mo molar ratio, 5 mmol of CuCl_2 was reacted with 0.714 mmol of $(\text{NH}_4)_6\text{Mo}_7\text{O}_{24} \cdot 4\text{H}_2\text{O}$, corresponding to 5 mmol of Mo species, considering that each mole of ammonium heptamolybdate contains seven moles of Mo. Since $(\text{NH}_4)_6\text{Mo}_7\text{O}_{24} \cdot 4\text{H}_2\text{O}$ contains seven molybdenum atoms

per formula unit, the required amount of precursor was calculated using the relation:

$$n(\text{AHM}) = n(\text{Mo}) / 7$$

Accordingly, for 5 mmol of Cu^{2+} , 0.714 mmol of ammonium heptamolybdate was used to maintain a 1:1 Cu:Mo molar ratio. This solution was stirred for 30 minutes at room temperature using a magnetic stirrer, then subjected to hydrothermal treatment at 150°C for 10 hours. The resulting particles were washed with deionized water and ethanol, then calcined at 500°C for 2 hours.

2.3. Synthesis of Acetylene Black

To synthesize acetylene black, concentrated hydrochloric acid (HCl) was added in equal volume to the graphite sample, and the mixture was stirred on a magnetic stirrer for 24 hours to ensure homogenization. The mixture was then washed several times with deionized water to remove excess HCl. After washing, the sample was dried at room temperature. To eliminate oily residues, it was treated with a benzene and acetone mixture in equal volumes. Following this step, the sample was filtered, dried again, and then heated in a vacuum furnace at 600°C for 24 hours to remove entrapped gases.

2.4. Structural Characterization

In supercapacitor cells, when optimal compatibility is achieved between the KOH electrolyte and electrode materials, initial studies are conducted using a three-electrode system. Following optimization based on these measurements, symmetric and asymmetric full cells are fabricated with the best-performing electrodes. The electrochemical properties of the supercapacitors are then analyzed using cyclic voltammetry (CV) and galvanostatic charge-discharge (GCD) techniques. The cycling stability, charge/discharge time, and specific capacitance of the supercapacitor cell are determined based on these measurements.

2.5. X-ray Diffraction (XRD)

X-ray diffraction (XRD) is one of the most widely used techniques for the characterization of nanoparticles. It is employed to determine a material's crystal structure, phase composition, lattice parameters, and crystallite size. XRD is based on the interaction between incident X-ray wavelengths and periodic structures within crystals; diffraction occurs when the X-ray wavelength is comparable to the periodic spacing of the crystal lattice. Crystals readily diffract X-rays with wavelengths matching their unit cell dimensions, though electrons or neutrons with appropriate energy can also be used.[23,24]

Since XRD patterns are sensitive to atomic arrangement and order, deviations from an ideal crystal structure—such as dislocations, internal stresses, or three-dimensional disorder can be observed as variations in diffraction peaks. In the absence of diffraction, incident X-rays are scattered in all directions. However, when diffraction occurs, constructive interference leads to

intensity maxima in specific directions and corresponding minima elsewhere.

Diffraction directions are typically described by the relationship between lattice planes. Bragg reflection occurs when the path difference between X-rays scattered by adjacent planes is an integer multiple of the wavelength (λ), as expressed in the Bragg equation:

$$n\lambda = 2d \sin \theta$$

where λ is the X-ray wavelength, n is an integer, θ is the angle of incidence, and d is the spacing between lattice planes. This equation relates the X-ray wavelength to the diffraction angle and interplanar spacing. Diffracted beams are detected, processed, and converted into intensity vs. 2θ patterns. Due to the random orientation of powder samples, scanning across a 2θ range captures all possible diffraction directions. The resulting d -spacings are compared to standard reference data (e.g., JCPDS) for phase identification [25-28].

In this thesis, XRD analysis was utilized to determine and confirm the chemical composition of the synthesized electrode materials.

2.6. Scanning Electron Microscopy (SEM) and Energy Dispersive X-ray Spectroscopy (EDX/EDS)

SEM and EDX are widely used techniques for structural and chemical characterization of supercapacitor electrode materials. SEM provides high-resolution images of the electrode surface, enabling evaluation of morphological parameters such as pore structure and particle size. EDX complements SEM by identifying the elemental composition of specific regions, providing insights into material homogeneity and the presence of impurities. Together, these techniques are critical for understanding factors that influence electrode performance.

EDX, used in conjunction with electron microscopy, identifies elements in a sample by detecting characteristic X-ray emissions. When combined with SEM, EDX enables elemental mapping and quantification of materials, including the analysis of heavy metal ions in closely packed nanoparticles. However, it has limitations in detecting elements with atomic numbers below 11 .

2.7. Fourier Transform Infrared Spectroscopy (FTIR)

FTIR spectroscopy is an effective and frequently used technique for identifying functional groups and chemical bonds in materials. Compared to traditional IR spectroscopy, FTIR provides faster and more accurate spectral data. In this method, infrared radiation emitted by a glowing blackbody source is spectrally encoded using a Michelson interferometer. Differences in optical path length create constructive and destructive interference, generating an interferogram.

This interferogram passes through the sample cell and interacts with the sample, absorbing IR radiation at frequencies specific to the sample's molecular structure. Vibrations that result in a change in dipole moment provide information about chemical bonds and functional

groups. The detector collects time-domain signals, including background noise. A Fourier transform algorithm is then used to extract the sample-specific IR spectrum by subtracting the background.

The most commonly observed vibrational modes in FTIR are stretching (ν), which involves changes in bond length, and bending (δ for in-plane, π for out-of-plane), which involves changes in bond angles. Polar functional groups (e.g., C=O, N–H, O–H) typically show strong and characteristic IR absorptions. The 1500–400 cm^{-1} range, known as the "fingerprint region," contains unique patterns useful for compound identification. Thus, FTIR enables detailed analysis of solid, liquid, and gaseous samples[29-31].

In this study, FTIR spectroscopy was employed to identify functional groups and chemical bonds in the synthesized materials.

2.8. Brunauer–Emmett–Teller (BET) Analysis

The surface of a nanomaterial contains a large proportion of atoms, which are key to determining its properties. Surface area measurement is essential for gaining insights into nanomaterials, and gas adsorption techniques are commonly used for this purpose. The BET method is one of the most widely applied techniques for surface area analysis. However, sample agglomeration can result in underestimation of surface area, so BET is typically performed on dry samples only.

In this study, BET analysis was used to determine the surface areas of the synthesized materials in order to interpret their electrochemical performance. Surface characteristics such as specific surface area and pore structure directly influence ion transport, active surface area, and overall performance in electrochemical applications.

BET analyses were conducted using a Micromeritics Gemini IV surface area analyzer. Specific surface areas were calculated based on nitrogen adsorption-desorption isotherms. Additionally, the Barrett–Joyner–Halenda (BJH) method was applied to evaluate pore volume and pore size distribution in detail. These measurements allowed for a more comprehensive understanding of the relationship between physical structure and electrochemical behavior.

2.9. Electrochemical Characterization

In this study, all electrochemical measurements were conducted at room temperature using a GAMRY Reference 3000 Potentiostat, which is illustrated in Figure 1.

This potentiostat functions by precisely controlling the potential between the reference and working electrodes, while supplying current through the counter electrode in order to maintain a stable potential at the working electrode.



Figure 1. GAMRY Reference 3000 potentiostat device

2.10. Electrode Fabrication and Tests

New-structured supercapacitor electrodes were prepared using nickel foam, as illustrated in Figure 2. Initially, the nickel foam was washed with 1 M hydrochloric acid (HCl) and the process was repeated 2–3 times, followed by drying in a vacuum oven. To prepare the electrode slurry, 85 wt% of active material (MMoO_4 , where $M = \text{Cu}$), 10 wt% activated carbon, and 5 wt% PVDF were placed into an appropriate glass beaker. N-methyl-2-pyrrolidone (NMP) was added for the first measurement and dimethyl sulfoxide (DMSO) for the second to form a slurry with suitable viscosity not too thick or too fluid.

The prepared mixture was subjected to ultrasonic treatment in a bath sonicator to ensure homogeneity of all components. The resulting uniform slurry was then applied to the surface of the nickel foam. The coated nickel foam electrodes were dried in a vacuum oven overnight and then made ready for electrochemical measurements. The working electrodes were fabricated by mixing CuMoO_4 active material, acetylene black, and polyvinylidene fluoride (PVDF) binder in a weight ratio of 80:10:10. The mixture was dispersed in N-methyl-2-pyrrolidone (NMP) to obtain a uniform slurry. The slurry was then coated onto pre-cleaned nickel foam ($1 \times 1 \text{ cm}^2$), followed by drying at 80 °C for 12 h under vacuum. The average mass loading of the active material was approximately 2.2 mg cm^{-2} . The specific capacitance was calculated based on the mass of the active material using the relation $C = (I \times \Delta t) / (m \times \Delta V)$.

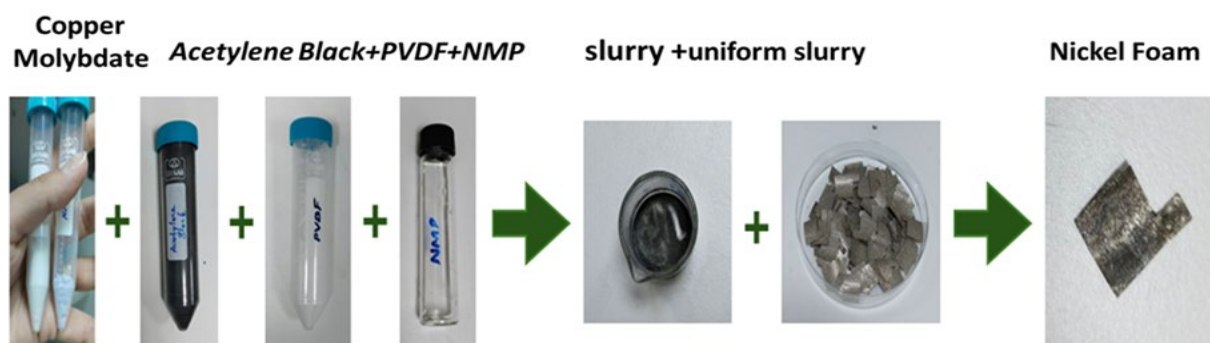


Figure 2. Supercapacitor electrodes prepared on a nickel foam substrate

2.11. Electrochemical Characterization of (CuMoO₄) Used in Supercapacitor Electrodes

In this study, the electrochemical performances of copper molybdate (CuMoO₄) based electrode materials for supercapacitor applications were evaluated using a three-electrode electrochemical cell system. The synthesized active materials were employed as the working electrodes and tested in a 2 M potassium hydroxide (KOH) aqueous electrolyte. An Ag/AgCl electrode was used as the reference electrode, while a platinum wire served as the counter (auxiliary) electrode. This three-electrode setup enabled a comprehensive analysis of the potential behavior and capacitance properties of each active material.

To ensure a reliable comparison among the molybdate-based electrode materials, all electrochemical tests were conducted under identical conditions. Cyclic voltammetry (CV) measurements were performed within a defined potential window of 0 V to 0.45 V, using scan rates ranging from 5 mV/s to 100 mV/s. These measurements provided insights into the charge storage behavior of the electrodes under both slow and fast scan rates. The resulting CV curves offered critical information regarding the electrochemical stability, reversibility, and capacitive properties of the materials [32-36].

Galvanostatic charge-discharge (GCD) tests were conducted at various current densities (A/g) to evaluate the specific capacitance behavior of the electrodes in detail. These measurements also enabled the monitoring of energy storage and release capacities over time. The specific capacitance values (Cs) were calculated using data obtained from the GCD curves, based on Equation 2. These Cs values serve as fundamental parameters in quantitatively assessing the energy storage performance of each electrode material.

Following these tests, electrochemical impedance spectroscopy (EIS) measurements were carried out to determine key parameters such as internal resistance components, charge transfer resistance, and ion diffusion behavior. EIS analysis was conducted over a broad frequency range (typically from 10⁵ Hz to 10⁻² Hz), and Nyquist plots were used to evaluate and deconvolute the resistance and capacitance contributions of the materials.

In conclusion, the electrochemical properties of CuMoO₄ was systematically compared under the same testing conditions. The energy storage potential of each material was thoroughly assessed, providing a critical dataset for evaluating the applicability of molybdate-based materials as promising electrode candidates for supercapacitor systems.

3. Results and Discussion

X-ray diffraction (XRD) analysis was performed to check the formation and phase character of the patterns. X-ray diffraction (XRD) analysis was performed using a Pan Analytical diffractometer equipped with Cu K α radiation ($\lambda = 1.5406 \text{ \AA}$). The measurements were carried out in the 2θ range of 10–80° with a scanning rate of 2° min⁻¹ and a step size of 0.02°. The instrument was operated at 40 kV and 40 mA. As shown in Figure 3, the XRD pattern of the synthesized CuMoO₄ sample exhibits distinct diffraction peaks at 2θ values of 18.91°, 31.24°, 36.60°, 38.31°, 44.70°, 55.29°, 59.09°, and 65.09°. These reflections can be indexed to the monoclinic CuMoO₄ phase according to the standard diffraction data (JCPDS No. 22-0604). The observed peaks correspond to the (-101), (101), (002), (020), (-202), (022), (-113), and (023) lattice planes, respectively. No additional impurity peaks were detected, confirming the successful formation of phase-pure monoclinic CuMoO₄.

The identified diffraction planes are consistent with the crystallographic characteristics of the monoclinic crystal system, validating the structural integrity of the synthesized CuMoO₄ material.

The dominant peaks observed in the XRD pattern, particularly at 31.24°, 36.60°, and 44.70°, indicate that the sample possesses a well-crystallized structure. This observation suggests that the synthesized material exhibits high purity and a well-ordered crystalline framework, which is critical for its functional performance. Furthermore, the position and intensity of these peaks provide strong evidence that the crystal structure of the CuMoO₄ phase has been successfully formed as intended.

This overlap was identified through comparison with the standard data provided in JCPDS card No. 73-1702. Although the synthesized material is primarily CuMoO_4 -based, it is well-documented in the literature that certain crystal planes of molybdate structures can produce diffraction patterns similar to those of monoclinic type structures[35].

Fourier Transform Infrared (FT-IR) spectroscopy was conducted to identify the functional groups and metal-oxygen bonds present in the CuMoO_4 sample (Figure 3). The resulting spectrum provides crucial insights into the molecular structure of the material. In the FT-IR spectrum, distinct absorption bands were observed in the range of 400–4000 cm^{-1} , corresponding to characteristic vibrational modes of the CuMoO_4 compound.

Strong absorption bands observed around 807 cm^{-1} and 895 cm^{-1} are attributed to the asymmetric and

symmetric stretching vibrations of Mo–O bonds. These bands confirm the presence of MoO_4^{2-} tetrahedral structural units and reflect the orderly arrangement of molybdenum-oxygen bonds within the crystal structure. Lower frequency bands in the range of 500–700 cm^{-1} are assigned to the vibrational modes of Cu–O bonds, indicating that Cu^{2+} ions are coordinated with oxygen atoms, thus confirming the successful formation of the CuMoO_4 compound [37].

Additionally, a broad absorption band observed around 3400 cm^{-1} is associated with surface-adsorbed –OH groups or moisture content. This suggests the presence of hydroxyl groups on the surface of the sample, which may contribute to its electrochemical activity. A weaker band near 1620 cm^{-1} is related to the bending vibrations of water molecules, indicating that the sample may have been slightly affected by ambient humidity.

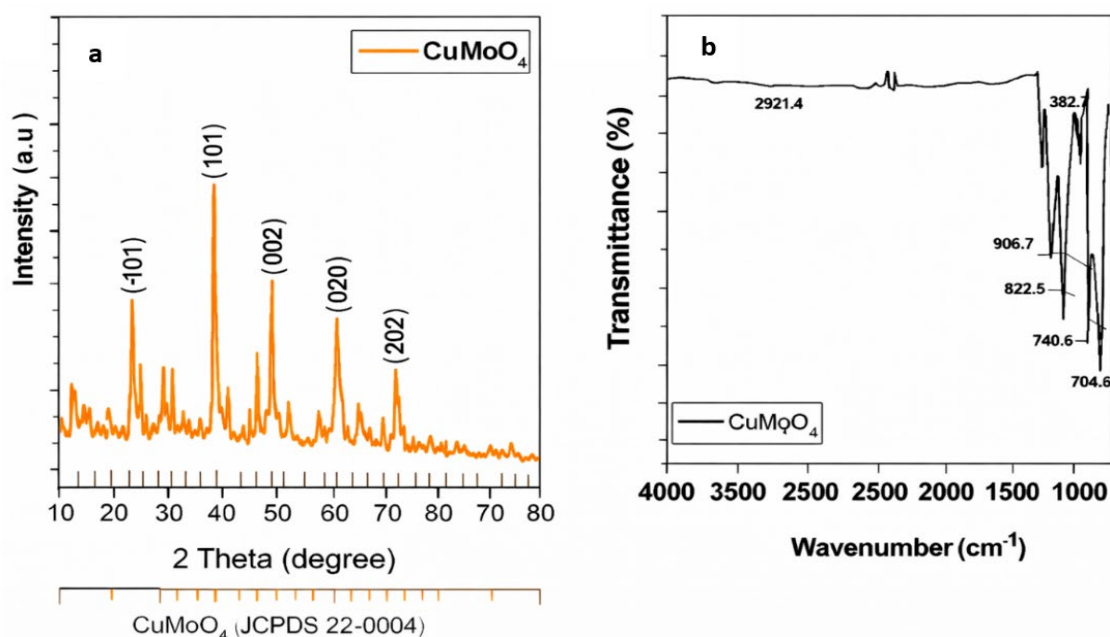


Figure 3. Structural characterization. (a) XRD patterns, and (b) FTIR spectra of CuMoO_4

The BET analysis was performed to evaluate the specific surface area and pore characteristics of the synthesized CuMoO_4 material. The nitrogen adsorption-desorption isotherm (Figure 4a) exhibits a type IV isotherm with a hysteresis loop, confirming the presence of mesoporosity. The specific surface area of the CuMoO_4 sample was determined to be 6.4592 $\text{m}^2 \text{g}^{-1}$. Although this value is relatively moderate, it is consistent with the compact rod-like morphology observed in FESEM images. The electrochemical performance is therefore expected to be governed not only by surface area but also by the material's intrinsic redox activity and pore architecture.

The BJH pore size distribution curve (Figure 4b) reveals a dominant pore size centered at approximately 16.59 nm (165.9 Å), with the majority of pores distributed within the 2–50 nm range. This clearly confirms the mesoporous nature of the CuMoO_4 material. The mesoporous structure facilitates electrolyte penetration and enhances ion diffusion pathways, thereby reducing diffusion resistance during charge-discharge processes. Such

structural characteristics are beneficial for improving electrochemical kinetics and overall energy storage performance. Although the surface area of the CuMoO_4 material is relatively low, its well-defined and appropriately sized pore structure can partially compensate for this limitation. The mesoporous structure is expected to facilitate ion transfer by providing active surface sites, making the material potentially functional in electrochemical applications. Furthermore, performance improvement may be achieved by synthesizing derivative structures or composite materials with higher surface areas [37]. BET analysis data reveal that the CuMoO_4 sample possesses a moderate surface area and a mesoporous structure that can be considered advantageous for electrochemical applications. Evaluating these properties in the context of electrochemical energy storage systems can provide valuable insights for developing synthesis strategies aimed at enhancing material performance.

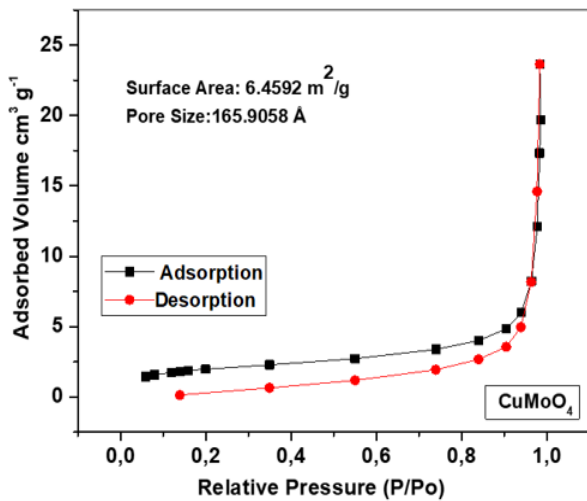


Figure 4. N_2 adsorption–desorption isotherm of $CuMoO_4$

To examine the surface morphology of the $CuMoO_4$ sample, Field Emission Scanning Electron Microscopy (FESEM) images were obtained at various magnifications (Figure 3.3) (10,000 \times , 20,000 \times , 30,000 \times , and 50,000 \times). These multi-scale magnifications allowed for a detailed microstructural analysis of the sample's surface. At lower magnifications (10,000 \times and 20,000 \times), the overall surface architecture could be observed, whereas at higher magnifications (30,000 \times and 50,000 \times), the morphological features, particle size distribution, and surface roughness became more pronounced. The images revealed a porous structure composed of irregularly shaped particles that are homogeneously distributed across the surface. This morphology is considered advantageous for energy storage applications, as it provides active surface area and facilitates ion transport. In addition to FESEM imaging,

Energy Dispersive X-ray Spectroscopy (EDX) analysis was conducted to support the morphological findings with elemental composition data. The EDX results (Figure 3.4) confirmed the presence of copper (Cu), molybdenum (Mo), and oxygen (O) in the sample and demonstrated their homogeneous distribution. The FESEM images (Figure 5) reveal that the synthesized $CuMoO_4$ exhibits a well-defined nanorod/nanoplatelet morphology rather than irregularly shaped particles. The structures appear as interconnected nanorods with elongated geometry, forming a porous and loosely packed architecture. The average diameter of the nanorods is approximately 100–200 nm, while their lengths extend up to several hundred nanometers. In addition, thin nanoplatelet-like features are observed, contributing to the hierarchical surface structure.

This distinct morphology provides a high electroactive surface area and facilitates efficient electrolyte penetration and ion diffusion, which is expected to enhance the electrochemical performance of the electrode material.

The observed elemental ratios were consistent with the expected stoichiometry of the $CuMoO_4$ compound. Furthermore, the absence of any extraneous elements indicates that the synthesis process was successfully performed with high chemical purity. The consistency between FESEM and EDX analyses strengthens the overall structural assessment. While FESEM confirmed the porous architecture that could enhance electrochemical performance, EDX verified the chemical integrity and purity of the $CuMoO_4$ structure. Taken together, these results indicate that the synthesized $CuMoO_4$ sample possesses the desired structural and compositional properties, making it a promising material for electrochemical applications[38].

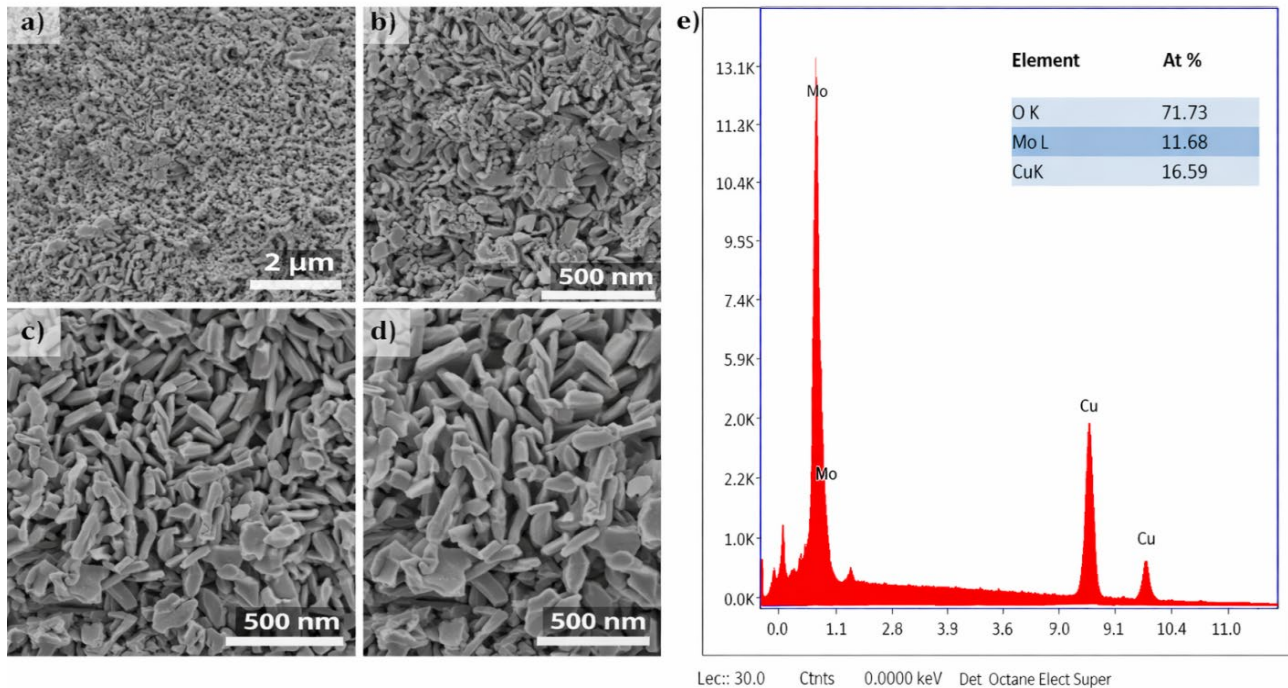


Figure 5. FESEM images of $CuMoO_4$ sample at different magnifications (a) 10,000 \times (b) 20,000 \times (c) 30,000 \times (d) 50,000 \times . (e) EDX analysis of the $CuMoO_4$

Comparison of CuMoO_4 in NMP and DMSO Solvents CuMoO_4 in NMP (*N*-Methyl-2-pyrrolidone)

Electrochemical characterization of the CuMoO_4 electrode prepared using NMP as a solvent was comprehensively investigated using three fundamental techniques: cyclic voltammetry (CV), galvanostatic charge-discharge (GCD), and electrochemical impedance spectroscopy (EIS). The graphical data corresponding to these analyses are presented in Figure 6 (a), (b), (c), and (d), respectively. Each of these techniques provides complementary insights into the energy storage mechanism, capacitance, and internal resistance behavior of the electrode[39].

In Figure 6 (a), the CV curves recorded at different scan rates within a potential window of 0–0.45 V demonstrate the capacitive behavior of the CuMoO_4 electrode. The broad and well-defined redox peaks observed in the CV curves clearly indicate the occurrence of Faradaic reactions at the electrode surface, confirming the pseudocapacitive nature of the CuMoO_4 structure. With increasing scan rates, the peak current also increases while maintaining the general shape of the curves, which suggests good electrochemical reversibility and rapid ion transport within the electrode material.

Figure 6 (b) shows the GCD curves obtained at various current densities, used to determine the specific capacitance of the CuMoO_4 electrode. The curves exhibit

a generally symmetrical profile, with comparable charge and discharge times, indicating a highly reversible energy storage behavior. The smooth and consistent GCD profiles reflect good electrochemical stability and uniform ion distribution across the active surface. These findings reveal that the material delivers higher specific capacitance values, particularly at lower current densities.

Figures 6 (c) and (d) present the EIS (Nyquist) plots used to evaluate the internal resistance (R_s) and charge transfer resistance (R_{ct}) of the electrode. The semicircle observed in the high-frequency region of the Nyquist plot corresponds to charge transfer resistance, and its relatively small diameter indicates a low R_{ct} value for the CuMoO_4 electrode. This suggests efficient charge transfer at the electrode–electrolyte interface and favorable electrochemical reaction kinetics. The linear slope in the low-frequency region represents the Warburg region associated with ion diffusion, and the observed slope confirms satisfactory ion conductivity within the CuMoO_4 electrode[38].

Overall, the CuMoO_4 electrode prepared in an NMP solvent medium exhibits pseudocapacitive characteristics, low internal resistance, and good electrochemical stability. The results from CV, GCD, and EIS analyses are consistent and mutually supportive, indicating that this electrode is a promising candidate for supercapacitor applications

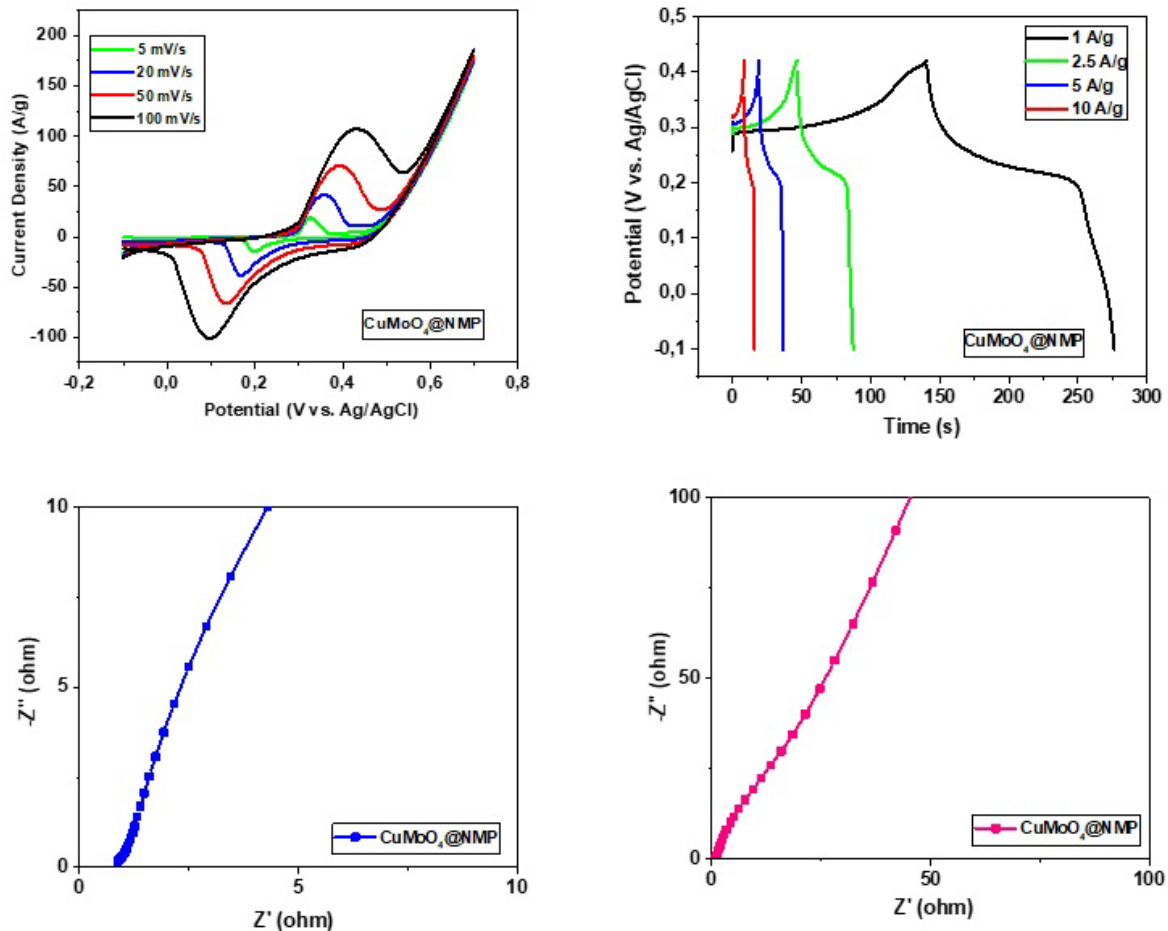


Figure 6. Electrochemical characterization of the CuMoO_4 electrode prepared using NMP as solvent:(a) Cyclic voltammetry (CV) curve(b) Galvanostatic charge-discharge (GCD) curve (c)-(d) Electrochemical impedance spectroscopy (EIS) Nyquist plots.

3.1. CuMoO_4 in DMSO (Dimethyl Sulfoxide)

The electrochemical properties of the CuMoO_4 active material-based electrode prepared using DMSO as a solvent were thoroughly investigated using a three-electrode system through cyclic voltammetry (CV), galvanostatic charge-discharge (GCD), and electrochemical impedance spectroscopy (EIS) techniques. The obtained data are presented in Figure 7 (a–d).

In Figure 7 (a), the CV curves were recorded in the potential range of 0–0.45 V at increasing scan rates. The presence of distinct oxidation and reduction peaks indicates that the CuMoO_4 electrode exhibits typical pseudocapacitive behavior. As the scan rate increases, both anodic and cathodic peak currents increase, while the general shape of the curves remains consistent. This observation reveals the good electrochemical reversibility of the electrode material and indicates that the CuMoO_4 electrode prepared in the DMSO medium contains homogeneously distributed active regions, allowing efficient ion transfer.

Figure 7 (b) displays the GCD curves obtained at different current densities, providing significant insights

into the charge storage capacity of the electrode. The curves exhibit a symmetric and smooth profile, demonstrating that the electrochemical processes are highly reversible and that energy losses occur at a minimal level. The close similarity between the charge and discharge times indicates high operational efficiency of the electrode. Moreover, the longer discharge times observed at lower current densities suggest that higher specific capacitance values can be achieved under these conditions.

The EIS analysis, shown in Figures 7 (c) and (d) through Nyquist diagrams, allowed the evaluation of the internal resistance and charge transfer characteristics of the CuMoO_4 electrode. The semicircle observed in the high-frequency region corresponds to the charge transfer resistance (R_{ct}), with a relatively small diameter. This indicates that charge transfer at the electrode-electrolyte interface occurs rapidly and that the electrode structure prepared in DMSO has good electrical conductivity. The sloped line in the low-frequency region represents the Warburg region, which is associated with ion diffusion, and the steepness of this line suggests that the CuMoO_4 structure is porous and allows effective ion diffusion[40].

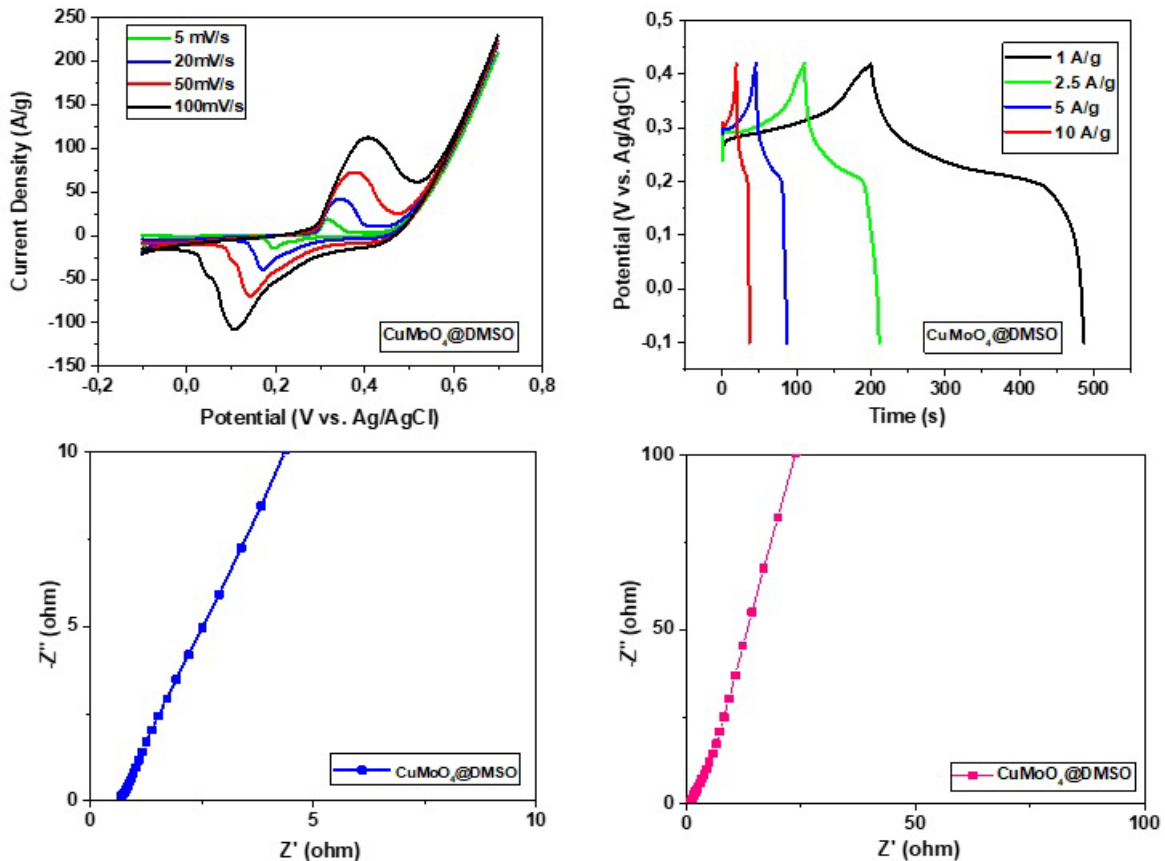


Figure 7. Electrochemical characterization of the CuMoO_4 electrode prepared with DMSO as the solvent: (a) CV curve, (b) charge-discharge (GCD) curve, (c)–(d) EIS Nyquist plots.

Table 1. Comparison of Specific Capacitances at Different Current Densities and Electrochemical Characterization Results of CoMoO₄ Electrodes Prepared Using NMP and DMSO Solvents

NMP	C1(F/g)	C2.5(F/g)	C5(F/g)	C10(F/g)	C20(F/g)	DÖNGÜ	CV(Volt)	GSD
CuMoO ₄	266	203.05	175.7	165	158	20A	-0.1/0.7	0.1/0.42
DMSO	C1	C2.5	C5	C10	C20	DÖNGÜ	CV	GSD
CuMoO ₄	549.6	481.7	414	356	323	40A	-0.1/0.7	0.1/0.42

In summary, the CuMoO₄ electrode prepared using DMSO as a solvent demonstrates enhanced electrochemical performance compared to the electrode synthesized with NMP. As presented in Table 1, the DMSO-based electrode delivers a significantly higher specific capacitance at all tested current densities, reaching 549.6 F g⁻¹ at 1 A g⁻¹, whereas the NMP-based electrode exhibits 266 F g⁻¹ under the same conditions. Even at higher current densities, the DMSO-derived electrode maintains 323 F g⁻¹ at 20 A g⁻¹, while the NMP counterpart decreases to 158 F g⁻¹, indicating superior rate capability and better capacitance retention.

Both electrodes were evaluated under identical electrochemical testing conditions, including the same potential window (-0.1 V to 0.7 V for CV) and comparable GCD voltage ranges (-0.1 V to 0.42 V). Furthermore, cycling stability measurements were conducted under consistent parameters to ensure a fair comparison. The improved performance of the DMSO-derived electrode is therefore attributed not to differences in operating voltage, but to enhanced electrochemical kinetics, reduced internal resistance, and more efficient ion diffusion facilitated by its optimized microstructure. The superior redox activity, lower internal resistance, and more symmetrical charge-discharge behavior observed in the DMSO-prepared electrode are likely attributable to better dispersion of active material and the formation of a more uniform and conductive film on the electrode surface. This homogeneity facilitates more efficient ion diffusion and charge transfer during operation, as also supported by EIS results[39].

In conclusion, while both solvents enable the synthesis of functional CuMoO₄ electrodes, DMSO clearly provides enhanced electrochemical characteristics, making it a more favorable medium for the development of high-performance pseudocapacitive supercapacitors.

4. Conclusion

This study focused on the comparative evaluation of CuMoO₄ electrodes synthesized using two different solvents, N-Methyl-2-pyrrolidone (NMP) and Dimethyl sulfoxide (DMSO), in terms of their structural, morphological, and electrochemical properties. While both solvents enabled the successful synthesis of CuMoO₄ with characteristic crystalline and morphological features, notable differences were observed in their electrochemical performances.

Electrochemical analyses including cyclic voltammetry (CV), galvanostatic charge-discharge (GCD), and electrochemical impedance spectroscopy (EIS)

demonstrated that electrodes prepared using DMSO exhibited significantly superior energy storage behavior compared to those synthesized with NMP. Specifically, DMSO-based electrodes achieved a much higher specific capacitance across all current densities, reaching 549.6 F/g at 1 A/g, which is more than double the capacitance obtained with NMP (266 F/g at 1 A/g). Even at higher current densities, DMSO-based electrodes maintained excellent capacitance retention (323 F/g at 20 A/g), confirming their robust rate capability.

Moreover, the DMSO-prepared electrode demonstrated better cyclic stability over 40 cycles, compared to 20 cycles for the NMP-based counterpart. The nearly identical CV voltage ranges and GCD profiles between both electrodes indicate consistent voltage operation, but the enhanced charge transport and ion diffusion in the DMSO electrode are attributed to improved electrolyte penetration and more uniform film formation, as supported by Nyquist plots.

In conclusion, CuMoO₄ exhibits promising pseudocapacitive behavior, and the choice of solvent plays a pivotal role in optimizing its electrochemical performance. The DMSO solvent significantly enhances the electrode's specific capacitance, rate performance, and cycling stability, making it a more suitable medium for high-performance supercapacitor applications. These findings underscore the critical importance of processing conditions particularly solvent selection in the design and development of next-generation energy storage materials.

Conflict of Interest

There are no conflicts of interest in this work.

Acknowledgments

The authors sincerely acknowledge the technical staff of ERNAM (Erciyes University Nanotechnology Research Center) and TAUM (Technology Research and Application Center) for their essential support in the characterization processes, which significantly contributed to the completion of this study.

References

- [1] Ahmed, S., Gondal, M. A., Khan, J. A., Almessiere, M. A., Baykal, A., & Ali, A. (2025). Comparative transition molybdates (xMoO₄ (x = Co, Mn, Ni, and Zn)) for high-performance supercapacitors. *Inorganic Chemistry Communications*, 178,114514. <https://doi.org/10.1016/j.inoche.2025.114514>

- [2] Ali, A., Chiang, Y. W., & Santos, R. M. (2022). X-ray diffraction techniques for mineral characterization: A review for engineers of the fundamentals, applications, and research directions. *Minerals*, 12(2), 205. <https://doi.org/10.3390/min12020205>
- [3] Ali, N., Manoharan, S., Pazhamalai, P., & Kim, S.-J. (2022). CuMoO₄ nanostructures: A novel bifunctional material for supercapacitor and sensor applications. *Journal of Energy Storage*, 52, 104784. <https://doi.org/10.1016/j.est.2022.104784>
- [4] Ali, Z., Iqbal, M. Z., & Hegazy, H. (2023). Recent advancements in redox-active transition metal sulfides as battery-grade electrode materials for hybrid supercapacitors. *Journal of Energy Storage*, 73, 108857. <https://doi.org/10.1016/j.est.2023.108857>
- [5] Ansari, M. Z., Ansari, S. A., & Kim, S.-H. (2022). Fundamentals and recent progress of Sn-based electrode materials for supercapacitors: A comprehensive review. *Journal of Energy Storage*, 53, 105187. <https://doi.org/10.1016/j.est.2022.105187>
- [6] Arumugam, G., Chettiannan, B., Mathan, S., Selvaraj, M., Assiri, M. A., & Rajendran, R. (2025). Better understanding of redox additives in aqueous electrolyte for electrochemical supercapacitors. *Journal of Energy Storage*, 121, 116595. <https://doi.org/10.1016/j.est.2025.116595>
- [7] Asim, N., Ahmadi, S., Alghoul, M. A., Hammadi, F. Y., Saeedfar, K., & Sopian, K. (2014). Research and development aspects on chemical preparation techniques of photoanodes for dye sensitized solar cells. *International Journal of Photoenergy*, 518156. <https://doi.org/10.1155/2014/518156>
- [8] Baig, M. M., Gul, I. H., Baig, S. M., & Shahzad, F. (2021). The complementary advanced characterization and electrochemical techniques for electrode materials for supercapacitors. *Journal of Energy Storage*, 44, 103370. <https://doi.org/10.1016/j.est.2021.103370>
- [9] Beyers, I., Bensmann, A., & Hanke-Rauschenbach, R. (2023). Ragone plots revisited: A review of methodology and application across energy storage technologies. *Journal of Energy Storage*, 73, 109097. <https://doi.org/10.1016/j.est.2023.109097>
- [10] Bhat, T. S., Patil, P. S., & Rakhi, R. B. (2022). Recent trends in electrolytes for supercapacitors. *Journal of Energy Storage*, 50, 104222. <https://doi.org/10.1016/j.est.2022.104222>
- [11] Cai, J., Wang, Y., Li, Q., Cui, L., Wu, J., Liu, Z., & Liu, J. (2025). DMSO-doped polymer hydrogel electrolyte-based freeze-resistant flexible supercapacitors with high capacitance retention at low temperatures. *Electrochimica Acta*, 530, 146136. <https://doi.org/10.1016/j.electacta.2025.146136>
- [12] Chernysh, O., Khomenko, V., Makyeyeva, I., & Barsukov, V. (2019). Effect of binder's solvent on the electrochemical performance of electrodes for lithium-ion batteries and supercapacitors. *Materials Today: Proceedings*, 6, 42–47. <https://doi.org/10.1016/j.matpr.2018.10.066>
- [13] Choudhary, G., Dhariwal, J., Saha, M., Trivedi, S., Banjare, M. K., Kanaoujiya, R., & Behera, K. (2024). Ionic liquids: Environmentally sustainable materials for energy conversion and storage applications. *Environmental Science and Pollution Research*, 31(7), 10296–10316. <https://doi.org/10.1007/s11356-023-30952-4>
- [14] Cui, M., & Meng, X. (2020). Overview of transition metal-based composite materials for supercapacitor electrodes. *Nanoscale Advances*, 2(12), 5516–5528. <https://doi.org/10.1039/D0NA00764A>
- [15] Dmitriev, D. S., Nashchekin, A. V., & Popkov, V. I. (2020). The interfacial surface of an electrode for a supercapacitor as a factor affecting the capacitance and energy density. *Applied Surface Science*, 501, 144216. <https://doi.org/10.1016/j.apsusc.2019.144216>
- [16] El Hayaoui, W., Tajat, N., Talebi, J., El Mouhri, W., Nadif, I., Idlahcen, A., Bougdour, N., Tamimi, M., Qourzal, S., Assabbane, A., & Bakas, I. (2025). Investigation of the electrocatalytic activity of metal molybdate MMoO₄ (M = Fe, Ni, and Zn) and the development of ZnMoO₄/S-rGO for electrochemical sensing. *Food Chemistry*, 486, 144651. <https://doi.org/10.1016/j.foodchem.2025.144651>
- [17] Eom, H., Kang, J., Jang, S., Kwon, O., Choi, S., Shin, J., & Nam, I. (2022). Evaluating the electrochemical properties of supercapacitors using the three-electrode system. *Journal of Visualized Experiments*, 179. <https://doi.org/10.3791/63177>
- [18] Farahpour, M., & Arvand, M. (2021). Single-pot hydrothermal synthesis of copper molybdate nanosheet arrays as electrode materials for high areal-capacitance supercapacitor. *Journal of Energy Storage*, 40, 102742. <https://doi.org/10.1016/j.est.2021.102742>
- [19] Forouzandeh, P., Kumaravel, V., & Pillai, S. C. (2020). Electrode materials for supercapacitors: A review of recent advances. *Catalysts*, 10(9), 969. <https://doi.org/10.3390/catal10090969>
- [20] Frackowiak, E., & Béguin, F. (2001). Carbon materials for the electrochemical storage of energy in capacitors. *Carbon*, 39(6), 937–950. [https://doi.org/10.1016/S0008-6223\(00\)00183-4](https://doi.org/10.1016/S0008-6223(00)00183-4)
- [21] Iro, Z. S., Subramani, C., & Dash, S. S. (2016). A brief review on electrode materials for supercapacitor. *International Journal of Electrochemical Science*, 11(12), 10628–10643. <https://doi.org/10.20964/2016.12.73>
- [22] Jalal, N. I., Ibrahim, R. I., & Oudah, M. K. (2021). A review on supercapacitors: Types and components. *Journal of Physics: Conference Series*, 1973(1), 012015. <https://doi.org/10.1088/1742-6596/1973/1/012015>
- [23] Jaleh, B., & Fakhri, P. (2016). Infrared and Fourier transform infrared spectroscopy for nanofillers and their nanocomposites. In S. Thomas, D. Rouxel, & D. Ponnamma (Eds.), *Spectroscopy of polymer nanocomposites* (pp. 112–129). <https://doi.org/10.1016/B978-0-323-40183-8.00005-9>
- [24] Jisha, M. R., Hwang, Y. J., Shin, J. S., Nahm, K. S., Kumar, T. P., Karthikeyan, K., Dhanikaivelu, N., Kalpana, D., Renganathan, N. G., & Stephan, A. M. (2009). Electrochemical characterization of supercapacitors based on carbons derived from coffee shells. *Materials Chemistry and Physics*, 115(1), 33–39. <https://doi.org/10.1016/j.matchemphys.2008.11.012>
- [25] Kang, C., Kim, C., Lee, S.-M., Liu, Y., & Kim, J.-K. (2025). Eco-friendly solvent alternative to N-methyl-2-pyrrolidone in lithium-ion battery electrode manufacturing. *Electrochimica Acta*, 526, 146209. <https://doi.org/10.1016/j.electacta.2025.146209>
- [26] Magar, H. S., Hassan, R. Y. A., & Mulchandani, A. (2021). Electrochemical impedance spectroscopy (EIS): Principles, construction, and biosensing applications. *Sensors*, 21(19), 6578. <https://doi.org/10.3390/s21196578>
- [27] Mendhe, A., & Panda, H. S. (2023). A review on electrolytes for supercapacitor device. *Discover Materials*, 3(1), 29. <https://doi.org/10.1007/s43939-023-00029-5>
- [28] Okafor, O. B., Popoola, A. P. I., Popoola, O. M., & Adeosun, S. O. (2025). Review on recent development of polyaniline and transition metal oxide composite electrode for supercapacitor application. *Next Materials*, 6, 100389. <https://doi.org/10.1016/j.nxmte.2025.100389>
- [29] Oyedotun, K. O., Ighalo, J. O., Amaku, J. F., Olisah, C., Adeola, A. O., Iwuozor, K. O., Akpomie, K. G., Conradie, J., & Adegoke, K. A. (2023). Advances in supercapacitor development: Materials, processes, and applications. *Journal of Electronic Materials*, 52(1), 96–129. <https://doi.org/10.1007/s11664-022-10152-1>
- [30] Pitcheri, R., Mooni, S. P., Sridhar, V., Radhalayam, D., Maaouni, N., Roy, S., Al-Zahrani, F. A. M., & Kummara, M.

- R. (2025). Ultra-small one-dimensional rice-like CoMoO_4 nanorods as a pseudocapacitive electrode. *Materials Science in Semiconductor Processing*, 185, 108865. <https://doi.org/10.1016/j.mssp.2025.108865>
- [31] Saliu, O. D., Iresemowo, O., Kubi, F., Moberuagba, K. H., Adeniyi, A. G., & Ramontja, J. (2025). Enhancing MoO_3 -based cathodes: Spinel CuMoO_3 vs non-spinel systems. *Journal of Materials Science: Materials in Engineering*, 20(1), 72.
- [32] Shanmugam, P., Hosomi, K., Rajendran, R., Krishnasamy, B., Kretkowski, M., Inami, W., Kawata, Y., & Dheivasigamani, T. (2024). Transition metal molybdate microstructures for supercapacitors. *Ceramics International*, 50(24), 55865–55878. <https://doi.org/10.1016/j.ceramint.2024.07.123>
- [33] Shariq, M., Alhashmialameer, D., Adawi, H., Alrahili, M. R., Almashnowi, M. Y. A., Alzahrani, A., Sharma, M., Ali, S. K., & Slimani, Y. (2025). Advancements in transition metal sulfide supercapacitors. *Journal of Industrial and Engineering Chemistry*, 144, 269–291. <https://doi.org/10.1016/j.jiec.2024.12.045>
- [34] Sharma, P., & Kumar, V. (2020). Study of electrode and electrolyte material of supercapacitor. *Materials Today: Proceedings*, 33, 1573–1578. <https://doi.org/10.1016/j.matpr.2020.05.123>
- [35] Sharma, S., & Chand, P. (2023). Supercapacitor and electrochemical techniques: A brief review. *Results in Chemistry*, 5, 100885. <https://doi.org/10.1016/j.rechem.2023.100885>
- [36] Shukla, U. (2025). Fourier transform infrared spectroscopy for nanomaterials. *Journal of Molecular Structure*, 1322, 140454. <https://doi.org/10.1016/j.molstruc.2025.140454>
- [37] Sing, K. S. W. (1985). Reporting physisorption data for gas/solid systems. *Pure and Applied Chemistry*, 57(4), 603–619. <https://doi.org/10.1351/pac198557040603>
- [38] Sliz, R., Valikangas, J., Santos, H. S., Vilmi, P., Rieppo, L., Hu, T., Lassi, U., & Fabritius, T. (2022). Suitable cathode NMP replacement for efficient sustainable printed Li-ion batteries. *ACS Applied Energy Materials*, 5(4), 4047–4058. <https://doi.org/10.1021/acsaem.1c02923>
- [39] Snook, G. A., Kao, P., & Best, A. S. (2011). Conducting polymer-based supercapacitor devices and electrodes. *Journal of Power Sources*, 196(1), 1–12. <https://doi.org/10.1016/j.jpowsour.2010.06.084>
- [40] Song, Y., Chen, Q., Zhang, H., Zhang, S., Zhang, K., Hu, J., Li, Y., & Yao, Y. (2025). Solvothermal method for preparing high-rate LiFePO_4 cathode material. *Materials Today Chemistry*, 45, 102659. <https://doi.org/10.1016/j.mtchem.2025.102659>